HOKKAIDO UNIVERSITY

Title	Transient analysis of oblique Hanle signals observed in GaAs
Author(s)	Lin, Zhichao; Kondo, Kenji; Yamamoto, Masafumi et al.
Citation	Japanese Journal of Applied Physics (JJAP), 55(4), 04EN03-1-04EN03-5 https://doi.org/10.7567/JJAP.55.04EN03
Issue Date	2016-04
Doc URL	https://hdl.handle.net/2115/64919
Rights	© 2016 The Japan Society of Applied Physics
Type	journal article
File Information	SS15196 - library.pdf

Hokkaido University Collection of Scholarly and Academic Papers : HUSCAP

Transient analysis of oblique Hanle signals observed in GaAs

Zhichao Lin,[1] Kenji Kondo,[2] Masafumi Yamamoto,[1] and Tetsuya Uemura[1,*]

[1]Division of Electronics for Informatics, Hokkaido University, Sapporo 060-0814, Japan
[2]Research Institute for Electronic Science, Hokkaido University, Sapporo 001-0020, Japan

A transient response of nuclear spins in GaAs to a change in a magnetic field was analyzed based on the time evolution of nuclear spin temperature. Simulation results well reproduced our experimental results on transient oblique Hanle signals observed in an all-electrical spin injection device, enabling a quantitative understanding of nuclear spin dynamics in the presence of a hyperfine interaction between nuclei and polarized electrons. Analysis regarding the time evolution of nuclear spin temperature revealed that the hysteretic nature of a nuclear field with respect to the sweep direction of an external field was caused by the delay of time response of nuclear spin temperature to a change in the magnetic field. This analysis provides a deep understanding of nuclear spin dynamics in semiconductors.

* uemura@ist.hokudai.ac.jp

1. Introduction

Spintronics, in which electron spins along with electron charges are used for information processing and memory, is an emerging technology for creating electronic devices with features of nonvolatility, reconfigurable logic functions, and ultralow power consumption, which are called spintronic devices. The understanding of the interplay between electron spins and nuclear spins due to the hyperfine interaction is a major issue in the development of spintronic devices. In the hyperfine interaction, non-equilibrium polarized electrons transmit their spin angular momentum to the lattice nuclei, leading to an effective nuclear spin polarization, referred to as dynamic nuclear polarization (DNP). The polarized nuclear spins will, in turn, affect the electron spins by enhancing electron spin relaxation in semiconductors [1]. Several instances of DNP in semiconductors induced by optical means or electrical means have been reported [2-17]. Furthermore, coherent manipulation of nuclear spins, or Rabi oscillation, which is a key factor for nuclear-spin-based qubits, has been demonstrated electrically in GaAs/AlGaAs quantum Hall systems [18-20] and optically in GaAs/AlGaAs quantum wells [21, 22]. In previous studies, we demonstrated high tunneling magnetoresistance (TMR) ratios of up to 1995% at 4.2 K and up to 354% at 290 K in magnetic tunnel junctions (MTJs) having Mn-rich Co_2MnSi electrodes [23], and 2610% at 4.2 K and 429% at 290 K in $Co_2(Mn,Fe)Si$ MTJs [24]. The obtained high TMR ratios for MTJs with Mn-rich Co_2MnSi or $Co_2(Mn,Fe)Si$ electrodes are attributed to suppressed Co_{Mn} antisites, which leads to the enhanced half-metallicity through a reduced density of minority-spin in-gap states around Fermi level [23-28]. The demonstration of high TMR ratios indicates a high spin polarization of Mn-rich Co_2MnSi or $Co_2(Mn,Fe)Si$. Thus, these Mn-rich Co-based Heusler alloys are promising spin source materials for a highly efficient spin injection into semiconductors. Indeed, we have demonstrated a high spin injection efficiency from Co_2MnSi into GaAs via an ultrathin insertion layer of CoFe in an all-electrical spin injection device, resulting in an electron spin polarization of up to 52% at the ferromagnetic/GaAs interface at 4.2 K [29]. Furthermore, we have demonstrated Rabi oscillation at a relatively low magnetic field of approximately 0.1 T in the same device [30].

The polarized nuclear spins affect electron spins as an effective magnetic field or Overhauser field. Thus, one can evaluate the degree of nuclear-spin polarization through the strength of the Overhauser field. To detect the nuclear field, oblique Hanle effect measurements have been widely used [2, 12-17]. While the electrical detection of oblique Hanle signals has been carried out only in a steady state in which the magnetic field was

swept slowly enough to ensure that the nuclear spin polarization was in equilibrium [14], we investigated the transient response of nuclear spins to a change in the magnetic field along with a time scale needed for DNP through transient oblique Hanle effect measurements in an all-electrical spin injection device with a Co_2MnSi spin source [17]. However, a rather complicated behavior of nuclear spins against a change in the magnetic field was observed, and only a qualitative understanding for this has been achieved. To fully exploit the nuclear spins in future spintronics, it is necessary to better understand the transient response of nuclear spins. In this paper, we quantitatively analyze the transient response of nuclear spins to a change in the magnetic field in the presence of a hyperfine interaction between nuclei and polarized electrons by using the concept of nuclear spin temperature.

2. Simulation model

Nuclear spins are coupled to each other by spin-spin interactions, and also loosely coupled to a lattice by a spin-lattice relaxation mechanism. The time scale for the spin-lattice system to reach thermodynamic equilibrium is characterized by T_1, which is on the order of 1 s or more. On the other hand, the interactions inside the nuclear spin system (dipole-dipole interaction of the nuclear magnetic moments) are characterized by a much shorter time, T_2. Each of the nuclei experiences a fluctuating local field B_L generated by its neighbors. The period of the nuclear spin precession in B_L defines the characteristic time of the interactions inside the nuclear spin system. Owing to these internal interactions, the nuclear spin system reaches the thermodynamic equilibrium internally during a time of order of T_2, which is given by $1/\gamma B_L$ and is generally on the order of 100 μs, where γ is the gyromagnetic ratio of nuclei. This equilibrium state is characterized by a nuclear spin temperature [31] which in general differs strongly from the lattice temperature because $T_1 >> T_2$. Based on Curie's law, the average nuclear spin $\mathbf{I_{av}^{(\alpha)}}$ and resultant Overhauser field $\mathbf{B_n}$ of all nuclei in the presence of an external magnetic field $\mathbf{B}$ are given by [32]

$$\mathbf{I}_{\mathrm{av}}^{(\alpha)} = \frac{(I_\alpha + 1)\mu_I^{(\alpha)}}{3k_B\theta_\alpha}\mathbf{B}, \tag{1}$$

$$\mathbf{B}_n = \sum_\alpha b_n^{(\alpha)}\mathbf{I}_{av}^{(\alpha)} / I_\alpha, \tag{2}$$

where α denotes the nuclei species, I_α is the value of nuclear spin, $\mu_I^{(\alpha)} = \gamma_\alpha \hbar I_\alpha$ is the nuclear magnetic moment, where $\hbar$ is the reduced Planck's constant, k_B is the Boltzmann constant, θ_α is the nuclear spin temperature, and $b_n^{(\alpha)}$ is the effective nuclear field at 100% nuclear

spin polarization. In the case of GaAs, the $b_n^{(\alpha)}$ (α = ^{75}As, ^{69}Ga, and ^{71}Ga nuclei) values are negative [32].

In the presence of polarized electrons, nuclear spins are effectively polarized through the transfer of spin angular momentum from polarized electrons to nuclei, leading to the cooling of nuclear spin temperature. The sign of the nuclear spin temperature is positive (negative) when the sign of $\mathbf{B}\cdot\mathbf{S}$ is positive (negative), where $\mathbf{S}$ is average electron spin ($|\mathbf{S}| = ½$, corresponding to 100% polarization). In the case that $\mathbf{B}\cdot\mathbf{S}$ is positive, the spin angular momentum parallel to $\mathbf{B}$ is transferred into the nuclear spin system, leading to an increased nuclear spin polarization. This corresponds to cooling of the nuclear spin temperature below the lattice temperature. For example, for $|\mathbf{S}| =0.25$ and $|\mathbf{B}| = 5$ mT, one finds $\theta_\alpha \sim 10^{-6}$ K. When $\mathbf{B}\cdot\mathbf{S}$ is negative, on the other hand, nuclear spins are negatively polarized because a population inversion occurs through the transfer of spin angular momentum antiparallel to $\mathbf{B}$, and the nuclear spin temperature becomes negative (see Fig. 1). However, the picture described above is the one for steady-state nuclear spins. If the external magnetic field is changed faster than the time scale of the DNP, the transient response of nuclear spins should be considered.

Considering the energy balance of the nuclear spin system interacting with polarized electrons, the time (t) evolution of nuclear spin temperature under the DNP process is described by the following equation [32]:

$$\frac{d}{dt}\left(\frac{1}{\theta_\alpha}\right) = -\frac{1}{T_{1e}}\left(\frac{1}{\theta_\alpha} - \frac{1}{\theta_{0\alpha}}\right), \tag{3}$$

where T_{1e} is the characteristic time for the DNP, which can be as long as 100 s or more, and $\theta_{0\alpha}$ is the steady-state nuclear spin temperature, which is given by [32]

$$\frac{1}{k_B\theta_{0\alpha}} = f_\alpha \frac{4I_\alpha}{\mu_I^{(\alpha)}} \frac{\mathbf{S}\cdot\mathbf{B}}{\mathbf{B}^2 + \xi B_L^2}, \tag{4}$$

where f_α (≤ 1) is the leakage factor, and ξ is a numerical coefficient defined by the ratio of the nuclear spin polarization rate to the depolarization rate [12]. The steady-state Overhauser field is characterized by $\theta_{0\alpha}$.

In the electrical oblique Hanle effect measurement using a four-terminal nonlocal geometry in a lateral spin transport device [Fig. 2(a)] [33-35], the Overhauser field can be detected through the detection of the nonlocal voltage V_{NL} between contacts 3 and 4. The total magnetic field of $\mathbf{B} + \mathbf{B_n}$ induces Hanle precession for electron spins, resulting in a decrease in the electron spin polarization under detector contact-3. Similarly to the conventional nonlocal Hanle signal, V_{NL} can be described by [36, 37]

$$V_{NL} = A\int_0^{\infty} \frac{1}{\sqrt{4\pi Dt}} \exp\left(-\frac{d^2}{4Dt}\right)\cos(\omega_L t)\exp\left(-\frac{t}{\tau_s}\right)\mathrm{d}t\,, \qquad (5)$$

where A is a constant, $D = l_{sf}^2/\tau_s$ is the diffusion constant, where l_{sf} is the spin diffusion length and τ_s is the electron spin relaxation time, d is the distance between contact-2 and contact-3, and $\omega_L = g\mu_B B_z/\hbar$ is the Larmor frequency, where B_z is the z component of $\mathbf{B} + \mathbf{B_n}$, g is an electron g-factor ($g = -0.44$ for GaAs), and μ_B is the Bohr magneton.

To simulate a transient oblique Hanle signal, we assumed an oblique magnetic field $\mathbf{B_{ob}}$, which was applied along the oblique direction with $\varphi = 15°$ from the z-axis in the x-z plane – *i.e.*, $\mathbf{B_{ob}} \equiv B_{ob}(\mathbf{x}\sin\varphi + \mathbf{z}\cos\varphi)$, where B_{ob} is the amplitude of the oblique field of $\mathbf{B_{ob}}$ with both the positive and negative signs, and $\mathbf{x}$ and $\mathbf{z}$ are the unit vectors along the x-axis and z-axis directions, respectively. The device was first initiated at B_{ob} = +42 mT for a hold time (t_{hold}) of 60 s, so that nuclear spins became dynamically polarized. Then B_{ob} was swept from +42 mT to –42 mT (negative sweep direction) and was swept back from –42 mT to +42 mT (positive sweep direction) with a sweep rate of 0.18 mT/s. In addition to $\mathbf{B_{ob}}$, we assumed a constant stray field B_{st} = 0.5 (mT) from the ferromagnetic electrodes, which pointed along the z-axis direction in the GaAs channel, as part of the external field in our simulation. Then, the total external magnetic field $\mathbf{B}$ was given by

$$\mathbf{B} = \mathbf{B_{ob}} + B_{st}\,\mathbf{z} = B_{ob}(\mathbf{x}\sin\varphi + \mathbf{z}\cos\varphi) + B_{st}\,\mathbf{z}\,, \qquad (6)$$

where B_{ob} as a function of t is given by

$$B_{ob}(t) = \begin{cases} 42 & (0 \le t \le 60) \\ 42 - 0.18(t-60) & \left(60 < t \le 60 + \dfrac{84}{0.18}\right) \\ -42 + 0.18\left(t - 60 - \dfrac{84}{0.18}\right) & \left(60 + \dfrac{84}{0.18} < t \le 60 + \dfrac{168}{0.18}\right) \end{cases}. \qquad (7)$$

From Eqs. (4), (6), and (7), $\theta_{0\alpha}$ in Eq. (3) is t-dependent. Thus, we solved Eq. (3) numerically by dividing t into a time step of 1 s, during which B_{ob} is assumed to be constant. Substituting numerically solved θ_α into Eqs. (1), (2), and (5), we simulated the transient response of $\mathbf{B_n}$ and V_{NL} against a change in the magnetic field.

Parameters used in our simulation are shown in Table I. The values of $2|\mathbf{S_0}|$, l_{sf}, and τ_{sf} in Table I were estimated from the fitting of our previous experimental results of the spin-valve signal (V_{NL} vs. in-plane magnetic field along the x-axis) and Hanle signals (V_{NL} vs. out-of-plane magnetic field) observed in a lateral spin transport device with Co_2MnSi/CoFe electrodes [17], where $|\mathbf{S_0}|$ is the average electron spin at $\mathbf{B} = \mathbf{0}$. These

results are shown in Figs. 2(b) and 2(c), respectively, and the details of the device structure and experimental conditions are described in Ref. 17. The projection of **S** to **B** in Eq. (4) was estimated from $|\mathbf{S_0}|$. Although the Hanle precession through **B** + $\mathbf{B_n}$ changes the component of **S** perpendicular to **B**, it does not change the component of **S** parallel to **B**. Thus, we assumed that $\mathbf{S}\cdot\mathbf{B}$ is equal to $\mathbf{S_0}\cdot\mathbf{B}$ in the simulation. We considered three kinds of nuclei ^{69}Ga, ^{71}Ga, and ^{75}As in the GaAs channel. The values of $b_n^{(\alpha)}$, T_{1e}, and f_α in Table I were treated as fitting parameters. The values of I_α and γ_α were taken from Ref. 38, and the value of $\sqrt{\xi}\,B_L$ was taken from Ref. 14.

3. Results and discussion

Fig. 3 shows (a) a typical oblique Hanle signal observed in GaAs with a Co_2MnSi spin source [17] and (b) a corresponding simulation result obtained using Eqs. (1)-(7). Compared with the simulated steady-state signal described in Ref. 17, we experimentally observed the following two features: (1) An additional side peak was observed at $B_{\rm ob} < 0$ in the negative sweep direction, and (2) no side peak was observed in the positive sweep direction, showing a clear hysteretic nature depending on the sweep direction. These features were well reproduced by using the concept of nuclear spin temperature. The value T_{1e} = 400 s used in the simulation is reasonable as a time scale needed for the DNP [12, 13, 17]. These results validate the simulation model used in this study. A slight deviation between the experiment and simulation for $B_{\rm ob} > 0$ is possibly due to the instability of the background signal during the measurement. Although we subtracted a background signal consisting of a constant term and linear and quadratic terms of $B_{\rm ob}$, some uncertain background signals might be remained.

Now we will discuss the transient behavior of nuclear spins based on the time evolution of nuclear spin temperature. Because $b_n^{(\alpha)}$ is negative in GaAs, we know from Eqs. (1) and (2) that if θ_α is positive (negative), $\mathbf{I_{av}}$ is parallel (antiparallel) to **B**, while $\mathbf{B_n}$ is antiparallel (parallel) to **B**. Thus, a condition that **B** and $\mathbf{B_n}$ cancel each other exists only for $\theta_\alpha > 0$. Fig. 4 shows (a) $B_{\rm ob}$, $B_{\rm n}$ and (b) $1/\theta_\alpha$, $1/\theta_{0\alpha}$ of ^{75}As nuclei as a function of time, and (c) a simulation result of an oblique Hanle signal, and Fig. 5 shows corresponding nuclear spin distribution of the transient oblique Hanle effect measurement. The value of $1/\theta_\alpha$ increased during a holding time due to DNP, resulting in the nuclear field $\mathbf{B_n}$ being generated antiparallel to **B** at $t = t_{\rm hold}$ [state-1 and Fig. 5(a)]. When $B_{\rm ob}$ reached 27 mT in the negative sweep direction, $\mathbf{B_n}$ and **B** cancelled each other out, leading to one side peak in the nonlocal voltage $V_{\rm NL}$ [state-2 and Fig. 5(a)]. When **B** was reversed, $\theta_{0\alpha}$ became negative

because $\mathbf{B}\cdot\mathbf{S} < 0$. This means that $\mathbf{B}$ and $\mathbf{B_n}$ should be parallel and no cancellation should occur in the steady state. However, we observed a clear side peak at B_{ob} = -11 mT [state-3 and Fig. 5(b)], indicating cancellation between $\mathbf{B}$ and $\mathbf{B_n}$. This is because $\mathbf{B_{ob}}$ was changed before the nuclear spin system reached the steady-state. Indeed, $1/\theta_\alpha$ was delayed with respect to $1/\theta_{0\alpha}$ as shown in Fig. 4(b), and θ_α stayed positive for a certain time after $\mathbf{B}$ was reversed. This time delay happened because the external magnetic field was changed much faster than T_1 and T_{1e} processes. After $\mathbf{B}$ was reversed, as shown in Fig. 5(b), the nuclear spin system adiabatically changed their spin direction to keep the Zeeman energy in the low-energy state for the negative B_{ob} as for the positive B_{ob}, resulting in a positive nuclear spin temperature. However, after sufficient time, that is, at t > 405 s, a population inversion of nuclear spins occurred owing to the DNP process and θ_α became negative, indicating $\mathbf{B_n}$ was parallel to $\mathbf{B}$ [state-4 and Fig. 5(c)]. Similarly in the positive sweep direction, θ_α was negative ($\mathbf{B}$ and $\mathbf{B}_{\mathrm{n}}$ were parallel) at $B_{\mathrm{ob}} < 0$, and it stayed negative for a certain time after $\mathbf{B}_{\mathrm{ob}}$ was reversed from the negative direction to the positive direction [state-5 and Fig. 5(d)]. Thus, no cancellation occurred between $\mathbf{B}$ and $\mathbf{B_n}$, resulting in the disappearance of the satellite peak at $B_{\mathrm{ob}} > 0$ for the positive sweep direction.

4. Conclusion

A transient response of nuclear spins in GaAs to a change in the magnetic field was analyzed by using the concept of nuclear spin temperature. The hysteretic nature of nuclear field with respect to the sweep direction of the external magnetic field, which originated from the transient response of nuclear spins, was well reproduced by this method. From the analysis, we found that this behavior can be understood by the delay of the time response of nuclear spin temperature to a change in the magnetic field. This finding contributes to a fuller understanding of nuclear spin dynamics.

Acknowledgement

This work was partly supported by JSPS KAKENHI Grant Numbers 25286039 and 15K13960.

References

[1] M. I. Dyakonov, in *Spin Physics in Semiconductors*, ed. M. I. Dyakonov (Springer, Heidelberg, 2008), Chap. 11.

[2] M. I. Dyakonov, V. I. Perel, V. L. Berkovits, and V. I. Safarov, Sov. Phys. JETP **40**, 950 (1975).

[3] D. Paget, G. Lampel, B. Sapoval, and V. I. Safarov, Phys. Rev. B **15**, 5780 (1977).

[4] G. Lampel, Phys. Rev. Lett. **20**, 491 (1968).

[5] J. Strand, B. D. Schultz, A. F. Isakovic, C. J. Palmstrøm, and P. A. Crowell, Phys. Rev. Lett. **91**, 036602 (2003).

[6] D. Gammon, S. W. Brown, E. S. Snow, T. A. Kennedy, D. S. Katzer, and D. Park, Science **277**, 85 (1997).

[7] G. Salis, D. T. Fuchs, J. M. Kikkawa, and D. D. Awschalom, Phys. Rev. Lett. **86**, 2677 (2001).

[8] T. Machida, T. Yamazaki, and S. Komiyama, Appl. Phys. Lett. **80** 4178 (2002).

[9] K. Hashimoto, K. Muraki, T. Saku, and Y. Hirayama, Phys. Rev. Lett. **88**, 176601 (2002).

[10] M. Poggio, G.M. Steeves, R. C. Myers, Y. Kato, A. C. Gossard, and D. D. Awschalom, Phys. Rev. Lett. **91**, 207602 (2003).

[11] K. Ono and S. Tarucha, Phys. Rev. Lett. **92**, 256803 (2004).

[12] J. Strand, X. Lou, C. Adelmann, B. D. Schultz, A. F. Isakovic, C. J. Palmstrøm, and P. A. Crowell, Phys. Rev. B **72**, 155308 (2005).

[13] P. Van Dorpe, W. Van Roy, J. De Boeck, and G. Borghs, Phys. Rev. B **72**, 035315 (2005).

[14] M. K. Chan, Q. O. Hu, J. Zhang, T. Kondo, C. J. Palmstrøm, and P. A. Crowell, Phys. Rev. B **80**, 161206(R) (2009).

[15] G. Salis, A. Fuhrer, and S. F. Alvarado, Phys. Rev. B **80**, 115332(R) (2009).

[16] J. Shiogai, M. Ciorga, M. Utz, D. Schuh, T. Arakawa, M. Kohda, K. Kobayashi, T. Ono, W. Wegscheider, D. Weiss, and J. Nitta, Appl. Phys. Lett. **101**, 212402 (2012).

[17] T. Akiho, J. Shan, H. -x. Liu, K. -i. Matsuda, M. Yamamoto, and T. Uemura, Phys. Rev. B. **87**, 235205 (2013).

[18] T. Machida, T. Yamazaki, K. Ikushima, and S. Komiyama, Appl. Phys. Lett. **82**, 409 (2003).

[19] G. Yusa, K. Muraki, K. Takashina, K. Hashimoto, and Y. Hirayama, Nature **434**, 1001 (2005).

[20] H. Takahashi, M. Kawamura, S. Masubuchi, K. Hamaya, T. Machida, Y. Hashimoto, and S. Katsumoto, Appl. Phys. Lett. **91**, 092120 (2007).

[21] H. Sanada, Y. Kondo, S. Matsuzaka, K. Morita, C.Y. Hu, Y. Ohno, and H. Ohno, Phys. Rev. Lett. **96**, 067602 (2006).

[22] Y. Kondo, M. Ono, S. Matsuzaka, K. Morita, H. Sanada, Y. Ohno, and H. Ohno, Phys. Rev. Lett. **101**, 207601 (2008).

[23] H. -x. Liu, Y. Honda, T. Taira, K. -i. Matsuda, M. Arita, T. Uemura, and M. Yamamoto, Appl. Phys. Lett. **101**, 132418 (2012).

[24] H. -x. Liu, T. Kawami, K. Moges, T. Uemura, M. Yamamoto, F. Shi, and P. M. Voyles, J. Phys. D: Appl. Phys. **48**, 164001 (2015).

[25] M. Yamamoto, T. Ishikawa, T. Taira, G. -f. Li, K. -i. Matsuda, and T. Uemura, J. Phys.: Condens. Matter **22**, 164212 (2010).

[26] G. -f. Li, Y. Honda, H. -x. Liu, K. -i. Matsuda, M. Arita, T. Uemura, M. Yamamoto, Y. Miura, M. Shirai, T. Saito, F. Shi, and P. M. Voyles, Phys. Rev. B **89**, 014428 (2014).

[27] J. -P. Wüstenberg, R. Fetzer, M. Aeschlimann, M. Cinchetti, J. Minár, Jürgen Braun, H. Ebert, T. Ishikawa, T. Uemura, and M. Yamamoto, Phys. Rev. B **85**, 064407 (2012).

[28] V. R. Singh, V. K. Verma, K. Ishigami, G. Shibata, T. Kadono, A. Fujimori, D. Asakura, T. Koide, Y. Miura, M. Shirai, G. -f. Li, T. Taira, and M. Yamamoto, Phys. Rev. B **86**, 144412 (2012).

[29] Y. Ebina, T. Akiho, H. -x. Liu, M. Yamamoto, and T. Uemura, Appl. Phys. Lett. **104**, 172405 (2014).

[30] T. Uemura, T. Akiho, Y. Ebina, and M. Yamamoto, Phys. Rev. B. **91**, 140410(R) (2015).

[31] A. Abragam and W. G. Proctor, Phys. Rev. **109**, 1441 (1958).

[32] M. I. Dyakonov and V. I. Perel, in *Optical Orientation*, ed. F. Meier and B. P. Zakharchenya (North-Holland, Amsterdam, 1984), Chap. 2.

[33] X. Lou, C. Adelmann, S. A. Crooker, E. S. Garlid, J. Zhang, S. M. Reddy, S. D. Flexner, C. J. Palmstrøm, and P. A. Crowell, Nat. Phys. **3**, 197 (2007).

[34] G. Salis, A. Fuhrer, R. R. Schlittler, L. Gross, and S. F. Alvarado, Phys. Rev. B **81**, 205323 (2010).

[35] M. Ciorga, A. Einwanger, U. Wurstbauer, D. Schuh, W. Wegscheider, and D. Weiss, Phys. Rev. B **79**, 165321 (2009).

[36] J. Fabian, A. Matos-Abiague, C. Ertler, P. Stano, and I. I. Zutic, Acta Phys. Slov. **57**, 565 (2007).

[37] I. Zutic, J. Fabian, and S. D. Samra, Rev. Mod. Phys. **76**, 323 (2004).

[38] D. Paget and V. L. Berkovits, in *Optical Orientation*, ed. F. Meier and B. P. Zakharchenya (North-Holland, Amsterdam, 1984), Chap. 9.

Figure Captions

Fig. 1. (Color online) Schematic images of nuclear spin distribution (a) under an external magnetic field, (b) under the DNP process when $\mathbf{B}\cdot\mathbf{S} > 0$, and (c) under the DNP process when $\mathbf{B}\cdot\mathbf{S} < 0$, where **S** is average electron spin.

Fig. 2. (Color online) (a) Schematic structure of a four-terminal nonlocal device and circuit configuration for oblique Hanle effect measurements. (b) Spin-valve signal and (c) Hanle signals observed in GaAs with a Co_2MnSi spin source. Reprinted with permission from Ref. 17. Copyright 2013, American Physical Society.

Fig. 3. (Color online) (a) Oblique Hanle signal observed in GaAs with a Co_2MnSi spin source. Reprinted with permission from Ref. 17. Copyright 2013, American Physical Society. (b) A corresponding simulation result obtained using Eqs. (1)-(7).

Fig. 4. (Color online) (a) Time evolution of (a) B_{ob} and B_n, (b) $1/\theta_\alpha$ and $1/\theta_{0\alpha}$ of ^{75}As isotope in GaAs. (c) A simulation result of oblique Hanle signal.

Fig. 5. (Color online) Schematic images of nuclear spin distribution of the transient oblique Hanle effect measurement for (a) state-1 and state-2, (b) state-3, (c) state-4, and (d) state-5.

Table I. Summary of simulation parameters.

Parameter	Value
$2\lvert\mathbf{S_0}\rvert$ (%)	4.4
τ_s (ns)	10
l_{sf} (μm)	5
b_n of ^{75}As (T)	-3.59
b_n of ^{69}Ga (T)	-2.19
b_n of ^{71}Ga (T)	-1.99
T_{1e} (s)	400
f_α	0.85
I_α [a)]	3/2
γ_α of ^{75}As [a)] [rad/(T·s)]	4.581×10^7
γ_α of ^{69}Ga [a)] [rad/(T·s)]	6.420×10^7
γ_α of ^{71}Ga [a)] [rad/(T·s)]	8.158×10^7
$\sqrt{\xi}\,B_L$ [b)] (mT)	5
d (μm)	0.5
B_{st} (mT)	0.5

a) Ref. 38. b) Ref. 14.

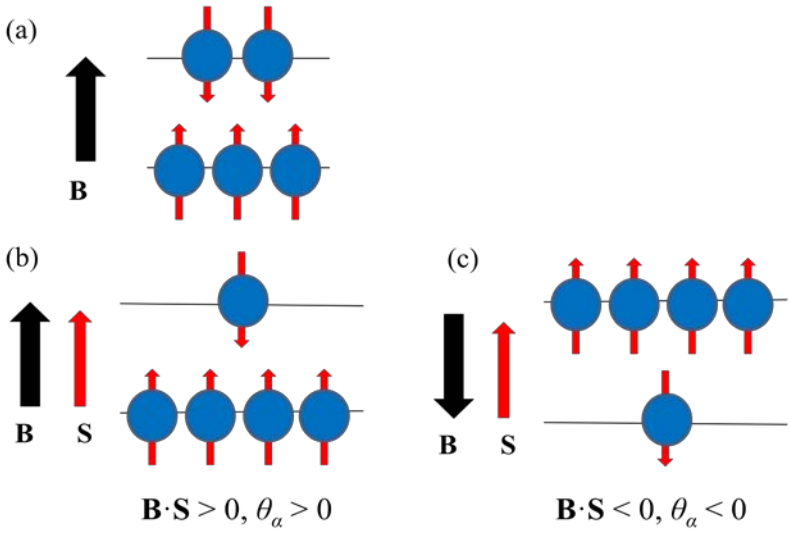

Fig. 1. (Color online) Schematic images of nuclear spin distribution (a) under an external magnetic field, (b) under the DNP process when **B**·**S** > 0, and (c) under the DNP process when **B**·**S** < 0, where **S** is average electron spin.

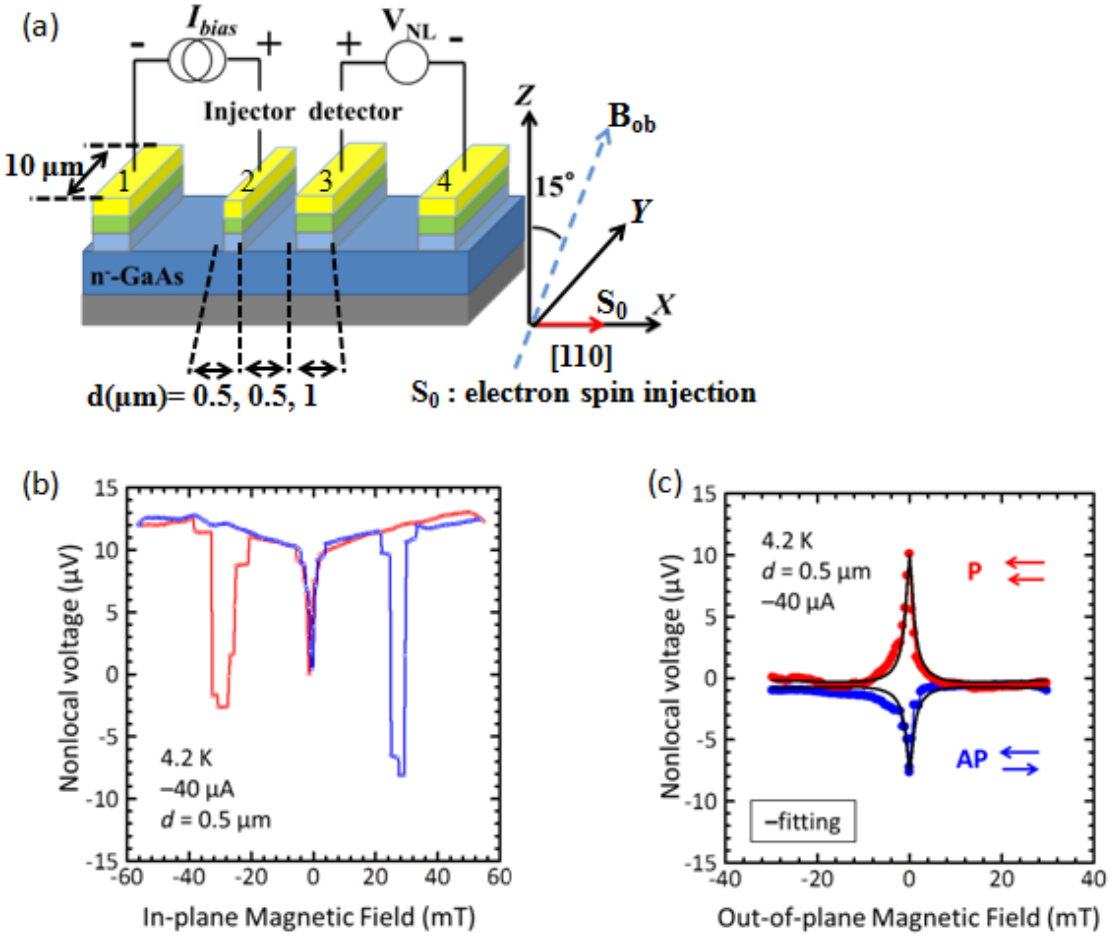

Fig. 2. (Color online) (a) Schematic structure of a four-terminal nonlocal device and circuit configuration for oblique Hanle effect measurements. (b) Spin-valve signal and (c) Hanle signals observed in GaAs with a Co_2MnSi spin source. Reprinted with permission from Ref. 17. Copyright 2013, American Physical Society.

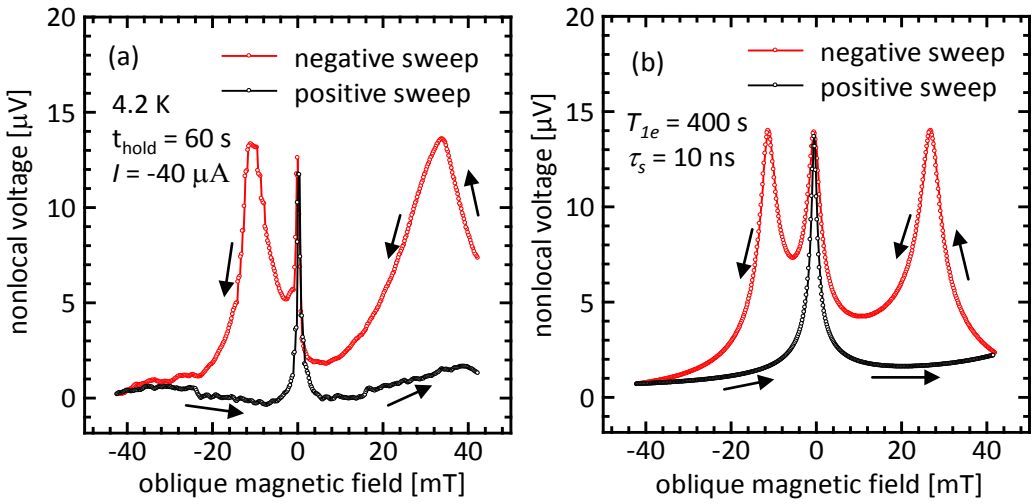

Fig. 3. (Color online) (a) Oblique Hanle signal observed in GaAs with a Co_2MnSi spin source. Reprinted with permission from Ref. 17. Copyright 2013, American Physical Society. (b) A corresponding simulation result obtained using Eqs. (1)-(7).

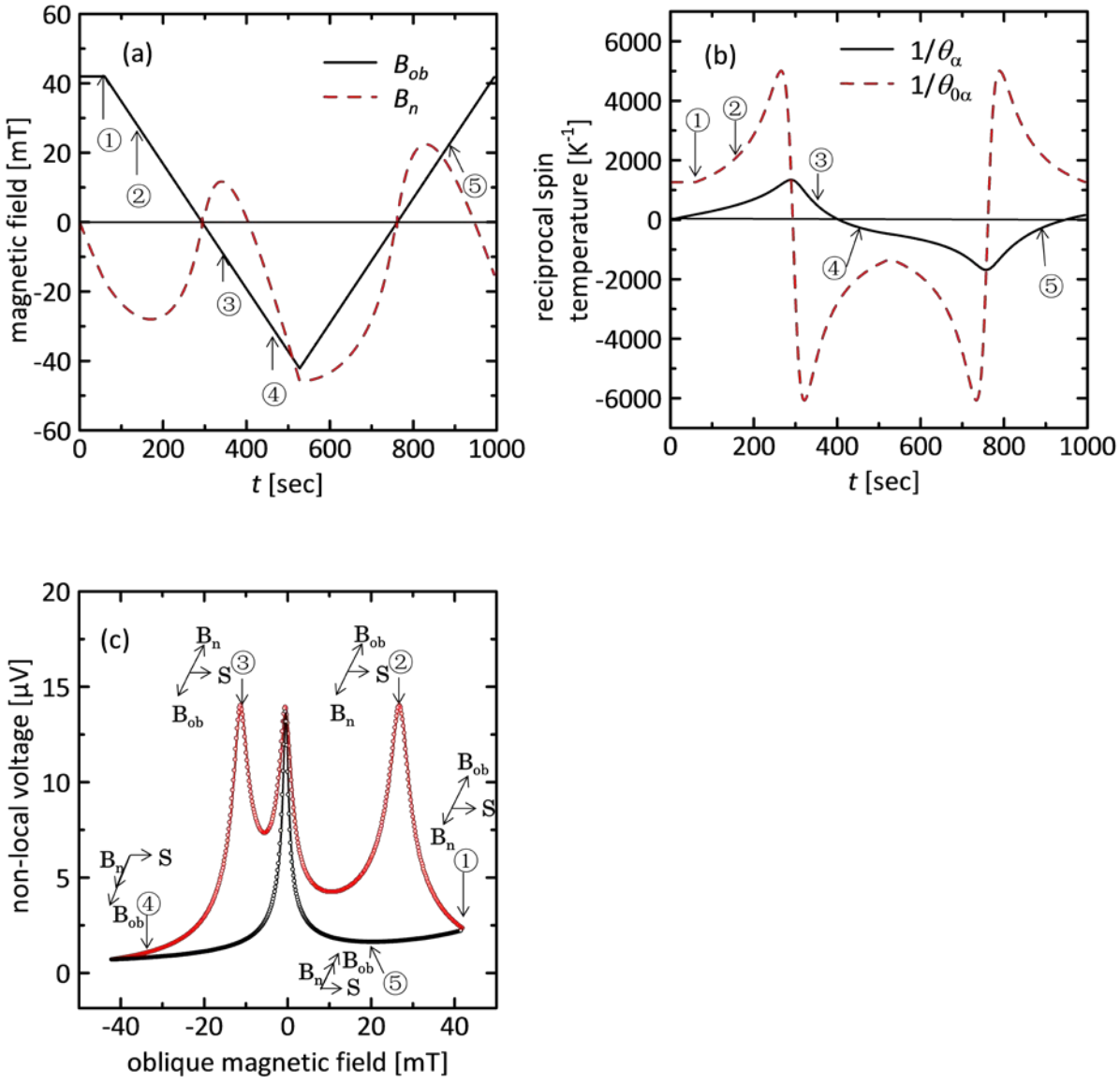

Fig. 4. (Color online) (a) Time evolution of (a) B_{ob} and B_n, (b) $1/\theta_\alpha$ and $1/\theta_{0\alpha}$ of ^{75}As isotope in GaAs. (c) A simulation result of oblique Hanle signal.

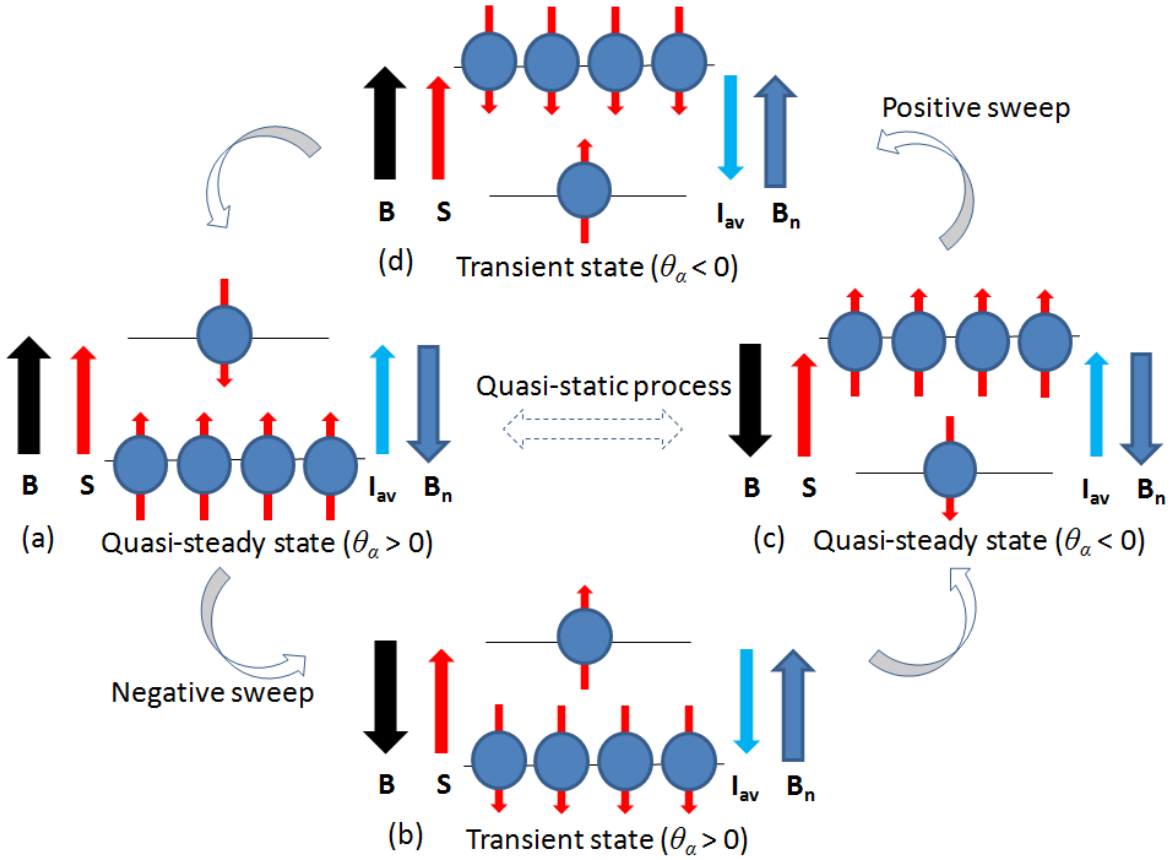

Fig. 5. (Color online) Schematic images of nuclear spin distribution of the transient oblique Hanle effect measurement for (a) state-1 and state-2, (b) state-3, (c) state-4, and (d) state-5.